Review

Nano Biomed Eng

Imaging-guided Companion Theranostics: Ushering in A New Era of Personalized Cancer Care

Meng Li[1,2], Yumeng Wu[1], Jing Lin[1]

[1] Marshall Laboratory of Biomedical Engineering, International Cancer Center, Laboratory of Evolutionary Theranostics (LET), School of Biomedical Engineering, Shenzhen University Medical School, Shenzhen University, Shenzhen 518055, China

[2] Nanophotonics Research Center, Shenzhen Key Laboratory of Micro-Scale Optical Information Technology, Institute of Microscale Optoelectronics, Shenzhen University, Shenzhen 518060, China

Corresponding author. E-mail: jingl@szu.edu.cn

Received: Nov. 12, 2024; **Revised:** Dec. 3, 2024; **Accepted:** Dec. 23, 2024

Citation: M. Li, Y.M. Wu, J. Lin. Imaging-guided companion theranostics: ushering in a new era of personalized cancer care. *Nano Biomedicine and Engineering*, 2025, 17(1): 3−16.

http://doi.org/10.26599/NBE.2025.9290112

Abstract

Tumor heterogeneity has increasingly underscored the urgent need for personalized medicine, prompting the Food and Drug Administration (FDA) to approve *in vitro* companion diagnostics (CDx) for patient stratification. This evolving landscape has gradually transitioned towards imaging-based CDx, which is now further integrated with therapeutic modalities, culminating in the emergence of companion theranostics (CTx). In this review, we systematically elucidate the development of CTx and provide the first formal definition of this concept, thereby establishing a clear framework that distinguishes it from existing diagnostic approaches. We particularly emphasize the design principles underlying CTx by introducing activation strategies that leverage tumor active markers and treatment-activation mechanisms to enhance therapeutic precision. Finally, we address key challenges that remain, including the markers discovery, fine-tuning probes design, and regulatory approvals for clinical applications. We hope the insights shared in this review will contribute to the design of CTx for oncology, advancing personalized medicine.

Keywords: companion diagnostics; companion theranostics; molecular imaging; patient identification; therapy prediction

Introduction

Tumor heterogeneity, a hallmark of cancer, presents significant challenges to effective treatment [1, 2]. The variability in genetic, molecular, and cellular characteristics of intra/inter tumors makes applying a one-size-fits-all therapeutic approach difficult. This heterogeneity underscores the critical need for personalized medicine, where treatments are tailored to the unique biological profile of each patient [3, 4]. Precision in patient selection becomes crucial to improving outcomes and minimizing side effects.

Clinical practice now largely depends on *in vitro* diagnostics (IVD) of biological samples to gather information that supports and/or guides the monitoring and prediction of therapeutic efficacy [5]. When these diagnostics are combined with FDA-approved treatments, they are referred to as companion diagnostics (CDx). Traditionally, CDx is a medical device, often *in vitro* biopsy-based analysis, used to stratify patients into subgroups based on their biomarker expression for approved drugs [6]. Although IVD-based CDx have proven valuable, they often fails to capture the dynamic and spatial

molecular profile of tumors.

With the continuous advancement of *in vivo* imaging technologies, such as positron emission tomography (PET), magnetic resonance imaging (MRI), and optical imaging, the field of personalized medicine has experienced a paradigm shift with the advent of molecular imaging-based CDx and, more recently, companion theranostics (CTx). Molecular imaging-based CDx acts as a non-invasive tool to visualize the tumor biomarker expression and changes, enabling clinicians to stratify patients for targeted therapy. CTx goes a step further by integrating CDx and therapeutic agents into a unified platform, enabling real-time monitoring and dynamic adjustment of treatments. In this review, we first define CTx as an integrated approach that combines therapy with imaging-based CDx, where therapy is simultaneously accompanied by a corresponding diagnostic to evaluate the therapy response for treatment prediction and guidance (Fig. 1). It is important to note that CTx differs from general theranostics in their primary focus. Traditional theranostics primarily emphasize the early detection of tumors and the immediate initiation of treatment. In comparison, CTx takes a more nuanced role by focusing on the continuous monitoring of the treatment process itself, rather than merely identifying the tumor at the onset.

Although there are already some reviews about CDx [7–9], most of them suffer from unclear classifications, failing to differentiate between CDx, CTx, and theranostics. This review addresses this gap by clearly defining CTx and systematically categorizing the relevant literature. We provide a comprehensive introduction to current molecular imaging-based CDx and CTx technologies, with a focus on design principles, application scenarios, and future directions. As the field progresses, the insights presented in this review will help drive more precise, tailored approaches to patient care, ultimately improving clinical outcomes.

State of the Art in CDx

Food and Drug Administration (FDA)-approved CDx

In 1998, the FDA approved trastuzumab in combination with HercepTest for the treatment of human epidermal growth factor receptor 2 (HER2)-positive metastatic breast cancer [10]. HercepTest is an immunohistochemistry (IHC) assay for HER2 detection. The simultaneous approval of trastuzumab and HercepTest was meaningful considering the tumor biomarker heterogeneity. This variability in tumor biomarkers, which can be receptors, signal proteins, or enzymes, affects how different patients respond to the same therapy, thus influencing both the success of targeted therapies and the potential for drug resistance. Since then, the FDA has adopted a policy of co-approving drugs and their corresponding diagnostics, and HercepTest has become the first FDA-approved CDx [6]. The FDA has identified several key scenarios where CDx should be applied, including identifying patients most likely to benefit or at risk of therapeutic products, monitoring responses, and predicting treatment efficacy for treatment adjustment. Until now, the FDA has approved 44 kinds of CDx to guide the selection of patient populations for various FDA-approved targeted

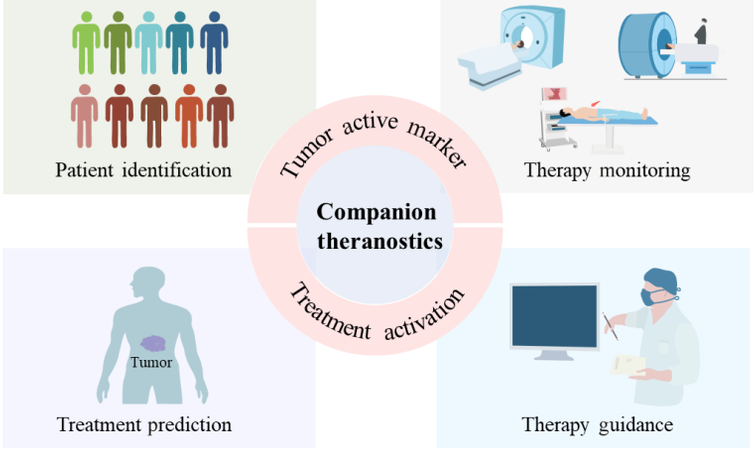

Fig. 1 Schematic illustration of the role of companion theranostics in patient identification, *in vivo* real-time therapy monitoring, therapy guidance, and treatment prediction.

drugs. Diseases covered by these approved CDx include multiple types of cancers (e.g., lung, breast, and colorectal cancer), myeloproliferative disorders, hemophilia, aggressive systemic mastocytosis, and so on. Our review primarily focuses on CDx related to tumors, and these approved CDx are summarized in

Table 1 FDA-approved CDx during1998–2024.

Disease	CDx	Associated biomarker	FDA-approved drugs
Non-small Cell Lung Cancer	Cobas EGFR Mutation Test v2	EGFR (HER1)	Tarceva, Tagrisso, Iressa, Gilotrif
	FoundationOne CDx	EGFR (HER1), ALK, BRAF, MET, BRAF, ROS1	Gilotrif, Iressa, Tarceva, Tagrisso, Alecensa, Xalkori, Zykadia, Tafinlar, Mekinist, Tabrecta, BRAFTOVI, Rozlytrek
	FoundationOne Liquid CDx	EGFR (HER1), BRAF, MET, ROS1, ALK	Iressa, Tagrisso, Tarceva, BRAFTOVI, MEKTOVI, Tabrecta, Alecensa
	Guardant360 CDx	EGFR (HER1), KRAS, ERBB2	Tagrisso, Rybrevant, Lumakras, ENHERTU
	ONCO/Reveal Dx Lung & Colon Cancer Assay	EGFR	Tyrosine kinase inhibitor
	Oncomine Dx Target Test	BRAF, ROS1, EGFR (HER1), RET	Tafinlar, Xalkori, Iressa, Gavreto, Rybrevant
	PD-L1 IHC 22C3 pharmDx	PD-L1	Keytruda, Libtayo, Opdivo
	therascreen EGFR RGQ PCR Kit	EGFR (HER1), KRAS	Gilotrif, Iressa, Gilotrif, Vizimpro, Lumakras, Krazati
	TruSight Oncology Comprehensive	RET	Retevmo
	Ventana ALK (D5F3) CDx Assay	ALK	Xalkori, Zykadia, Alecensa, Lorbrena
	Ventana PD-LI (SP263) Assay	PD-L1	Tecentriq
	Vysis ALK Break Apart FISH Probe Kit	ALK	Xalkori, Alunbrig
	Agilent Resolution ctDx FIRST assay	KRAS	Krazati
	Abbott RealTime IDH1	IDH1, IDH2	Tibsovo, Rezlidhia, Idhifa
Breast Cancer	Bond Oracle HER2 IHC System	ERBB2 (HER2)	Herceptin
	BRACAnalysis CDx	BRCA1 and BRCA2	Lynparza, Talzenna
	FoundationOne CDx	ERBB2 (HER2) PIK3CA	Herceptin, Perjeta, Kadcyla, Piqray, TRUQAP
	FoundationOne Liquid CDx	PIK3CA	Piqray
	Guardant360 CDx	ESR1	Orserdu
	HER2 CISH pharmDx Kit	ERBB2 (HER2)	Herceptin, Perjeta, Kadcyla
	HercepTest	ERBB2 (HER2)	Herceptin, Perjeta, Kadcyla
	INFORM HER-2/neu	ERBB2 (HER2)	Herceptin
	InSite Her-2/neu	ERBB2 (HER2)	Herceptin
	PathVysion HER-2 DNA Probe Kit	ERBB2 (HER2)	Herceptin
	PATHWAY anti-Her2/neu (4B5) Rabbit Monoclonal Primary Antibody	ERBB2 (HER2)	Kadcyla, Enhertu
	SPOT-LIGHT HER2 CISH Kit	ERBB2 (HER2)	Herceptin
	therascreen PIK3CA RGQ PCR Kit	PIK3CA	Piqray
	Ventana HER2 Dual ISH DNA Probe Cocktail	ERBB2 (HER2)	Herceptin
Myeloid Leukemia	LeukoStrat CDx FLT3 Mutation Assay	FLT3 (ITD/TDK)	Rydapt, Xospata, VANFLYTA,
	MRDx BCR-ABL Test	Philadelphia chromosome	Tasigna
Pancreatic Cancer	BRACAnalysis CDx	BRCA1 and BRCA2	Lynparza
Melanoma	cobas 4800 BRAF V600 Mutation Test	BRAF	Zelboraf, Cotellic
	FoundationOne CDx	BRAF	Mekinist, Tecentriq
	SeCore CDx HLA Sequencing System	HLA	Kimmtrak
	THXID BRAF Kit	BRAF	Tafinlar, Mekinist, Braftovi

(To be continued on the next page)

Table 1 (*Continued*)

Disease	CDx	Associated biomarker	FDA-approved drugs
Ovarian Cancer	BRACAnalysis CDx	BRCA1 and BRCA2	Lynparza, Rubraca
	FoundationFocus CDxBRCA Assay	BRCA1 and BRCA2	Rubraca
	Myriad myChoice CDx	Myriad HRD	Lynparza
	Ventana FOLR1 (FOLR-2.1) RxDx Assay	FOLR1	Elahere
	FoundationOne CDx	BRCA1 and BRCA2	Lynparza
Colorectal Cancer	cobas KRAS Mutation Test	KRAS	Erbitux, Vectibix
	CRCDx RAS Mutation Detection Assay Kit	KRAS and NRAS	Vectibix
	Dako EGFR pharmDx Kit	EGFR (HER1)	Vectibix, Erbitux
	FoundationOne Liquid CDx	BRAF	BRAFTOVI
	FoundationOne CDx	KRAS and NRAS	Erbitux, Vectibix
	ONCO/Reveal Dx Lung & Colon Cancer Assay	KRAS	Erbitux, Vectibix
	xT CDx	KRAS and NRAS	Erbitux, Vectibix
	therascreen BRAF V600E RGQ PCR Kit	BRAF	Braftovi
	therascreen KRAS RGQ PCR Kit	KRAS	Vectibix, Erbitux
Cholangiocarcinoma	FoundationOne CDx	FGFR2	Pemazyre
	Oncomine Dx Target Test	IDH1	Tibsovo
	FoundationOne CDx	TMB, MSI-High, RET, NTRK1, NTRK2 and NTRK3	Keytruda, Vitrakvi, Keytruda, RETEVMO, Rozlytrek,
Thyroid Cancer	Oncomine Dx Target Test	RET, BRAF	Retevmo, Tafinlar
Cervical Cancer	PD-L1 IHC 22C3 pharmDx	PD-L1	Keytruda
Solid Tumor	TruSight Oncology Comprehensive	NTRK1, NTRK2, and NTRK3 fusions	Vitrakvi
	Ventana MMR RxDx Panel	dMMR	Jemperli, Keytruda
Prostate Cancer	FoundationOne CDx	BRCA1 and BRCA2, HRR genes	AKEEGA, Lynparza
	FoundationOne Liquid CDx	BRCA1, BRCA2 and ATM	Rubraca, Lynparza
	BRACAnalysis CDx	BRCA1 and BRCA2	Lynparza
Gastric and Gastroesophageal Cancer	HER2 FISH pharmDx Kit	ERBB2 (HER2)	Herceptin
	HercepTest	ERBB2 (HER2)	Herceptin
	PD-L1 IHC 22C3 pharmD	PD-L1	Keytruda
Head and Neck Squamous Cell Carcinoma	PD-L1 IHC 22C3 pharmDx	PD-L1	Keytruda
Esophageal Squamous Cell Carcinoma	PD-L1 IHC 22C3 pharmDx	PD-L1	Keytruda
Urothelial Cancer	therascreen FGFR RGQ RT-PCR Kit	FGFR3	Balversa
Gastrointestinal Stromal Tumors	therascreen PDGFRA RGQ PCR Kit	PDGFRA	AYVAKIT
Endometrial Carcinoma	Ventana MMR RxDx Panel	deficient mismatch repair proteins	Jemperli, Keytruda
Urothelial Carcinoma	Ventana PD-L1 (SP142) Assay	PD-L1	Tecentriq
B-cell Chronic Lymphocytic Leukemia	Vysis CLL FISH Probe Kit	TP53	Venclexta

Note: EGFR: epidermal growth factor receptor; BRAF: B-Raf proto-oncogene; MET: mesenchymal-epithelial transition factor; KRAS: kirsten rat sarcoma viral oncogene homolog; RET: rearranged during transfection proto-oncogene; ERBB2: Erb-B2 receptor tyrosine kinase 2; PD-L1: programmed cell death 1 ligand 1; IDH: isocitrate dehydrogenase; BRCA: breast cancer susceptibility genes; PIK3CA: phosphatidylinositol 3-kinase; ESR1: estrogen receptor 1; FLT3: FMS-like tyrosine kinase 3; HRD: homologous recombination repair; FOLR1: folate receptor 1; HLA: human leukocyte antigen; NRAS: neuroblastoma RAS viral oncogene homolog; FGFR: fibroblast growth factor receptor; NTRK: neurotrophic receptor tyrosine kinase; dMMR: deficient mismatch repair; PDGFRA: platelet-derived growth factor receptor alpha; TP53: tumor protein p53.

Table 1.

Approved CDx primarily utilizes IVD methods, such as IHC and polymerase chain reaction (PCR), which are commonly used to detect specific genetic markers associated with a patient's response to targeted therapies [11]. However, IVD requires invasive procedures such as biopsies, which only provide a limited snapshot of a tumor's molecular profile. Moreover, the variation in biomarker expression within different regions of a tumor or between metastatic sites can further complicate the reliability of IVD results. Luckily, in 2013, the FDA approved FerriScan as a CDx imaging tool to support the use of Deferasirox, a drug for treating iron overload. FerriScan provides a non-invasive R2*-MRI method to accurately measure liver iron concentration, making it a valuable asset in monitoring patients' iron levels and assessing their response to iron-chelation therapies [12].

Imaging-based CDx

Imaging-based CDx is used to identify and monitor disease states, predict therapeutic responses, and assess treatment efficacy. Molecular design principles for imaging-based CDx are focused on creating probes that enable targeted, high-contrast, and reliable visualization of disease biomarkers *in vivo*. It generally includes three main components: a targeting moiety that specifically binds to disease biomarkers, an imaging or reporting unit that produces a detectable signal (such as fluorescence or radioactivity), and usually a linker that connects these components and may activate in specific environments to enhance accuracy. With ongoing advancements, many clinical studies have been conducted on imaging-based CDx, as summarized in Table 2.

Molecular imaging-based CDx has encompassed various imaging techniques such as MRI [13, 14], PET [15], single-photon emission computed tomography (SPECT) [16], and so on. Each imaging modality offers distinct advantages, enabling real-time, highly sensitive monitoring of biomarkers, and facilitating personalized treatment plans.

In the context of molecular imaging-based CDx, PET stands as the most paramount imaging modality due to its exceptional sensitivity and ability to monitor metabolic activity. It offers detailed visualization of internal molecular and cellular activities, making it crucial for early diagnosis and monitoring treatment response [10]. The design of PET-based CDx tools often involves the conjugation of PET tracers with antibodies, enhancing the specificity of the imaging. This method, known as immuno-PET, allows for targeted imaging of specific biomarkers associated with tumors, improving the accuracy of diagnostics. For example, Flamen et al. advanced the PET imaging-based CDx into a clinical study by conducting the ZEPHIR trial [17]. In this trial, PET tracer ^{89}Zr was conjugated with trastuzumab to sketch the HER2 expression. 57 patients with HER2-positive metastatic breast cancer underwent PET imaging before trastuzumab emtansine (T-DM1) treatment. The results demonstrated that tumors with uniform HER2 expression were more likely to respond well to T-DM1. Further combining HER2-PET/CT with FDG-

Table 2 Currently clinical trials on imaging-based CDx.

CDx Agent	Disease	Trial phase	NCT identifier	Status	Imaging modalities
^{89}Zr Crefmirlimab Berdoxa	Melanoma	Phase I	NCT05279027	Active, by invitation	PET/CT
^{68}Ga-grazytracer	Solid tumor	Phase I/ II	NCT05000372	Completed	PET/CT
Fluciclovine ^{18}F	Prostate cancer	Phase II	NCT03707184	Completed	PET/CT
^{18}F-ASIS	Breast cancer	Phase I	NCT03790423	Completed	PET/CT
^{89}Zr-DFO-SHR1920	Pancreatic cancer	Phase I	NCT06602037	Active, recruiting	PET/CT
[^{18}F]-ALF-FAPI-74	Colorectal cancer	Not Applicable	NCT06191120	—	PET/CT
Fluorine ^{18}F Ara-G	Urothelial carcinoma	Phase II	NCT03007719	Completed	PET/MRI
^{18}F-DCFPyL-iPSMA/^{68}Ga-HBED-iPSMA	Prostate cancer	Phase I	NCT04030338	Active, not recruiting	PET/CT
^{64}Cu-LNTH-1363S	Gastrointestinal tract cancer	Phase I/ II	NCT06298916	Active, recruiting	PET/CT
^{99m}Tc-EC0652	Prostate cancer	Phase I	NCT02202447	Completed	SPECT/CT
^{99m}Tc-etarfolatide	Non-small cell lung cancer	Phase II	NCT01577654	Completed	CT/MRI

PET/CT accurately predicted morphological response, distinguishing between patients with a median time-to-treatment failure (TTF) of just 2.8 months and those with a TTF of 15 months. These findings of the ZEPHIR trial suggested that ^{89}Zr-labeled trastuzumab PET imaging could serve as a CDx tool to identify HER2 heterogeneity between patients, which can affect the success of targeted therapies. In another case, Li et al. developed the ^{68}Ga-grazytracer, a probe targeting granzyme B, and conducted a phase I/II clinical trial (NCT05000372) involving 24 cancer patients to test its predictive value [18]. In patients with follicular lymphoma, ^{68}Ga-grazytracer PET showed high uptake post-therapy, indicating a favorable immune response, resulting in a complete metabolic response after 14 months (Figs. 2(a)–2(d)). In contrast, patients with B-cell lymphoma showed no tracer activity, correlating with poor prognosis and disease progression, which was confirmed by substantially increased ^{18}F-FDG uptake after 3 months (Figs. 2(e)–2(h)). These findings suggest ^{68}Ga-grazytracer's potential in enhancing immunotherapy assessment, patient stratification, and treatment planning.

Single-photon emission computed tomography (SPECT) also provides functional information at molecular levels, making it highly useful for detecting abnormalities in CDx. Although it has lower sensitivity and spatial resolution, it surpasses PET in terms of cost-effectiveness, wider availability, and broader ranges of tracers. SPECT employs various radionuclides, with the most commonly used ones being ^{99m}Tc, ^{67}Ga, ^{123}I, ^{125}I, ^{131}I, and ^{111}In. Wang Fan group has modified ^{99m}Tc with various antibodies, proteins, and peptides for CDx. For example, PD-L1-targeted nanobody MY1523 was radiolabeled with

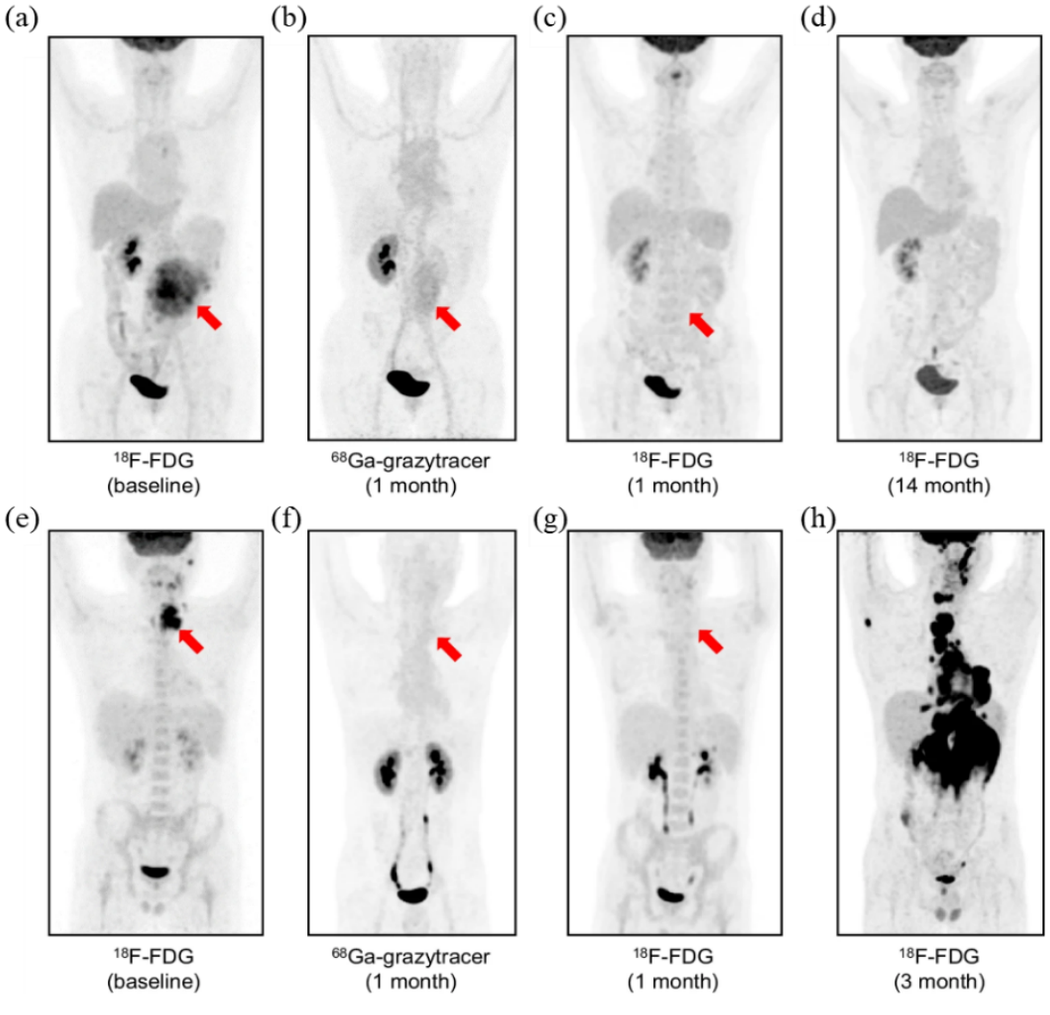

Fig. 2 A patient with follicular lymphoma underwent an initial **(a)** ^{18}F-FDG scan before treatment, **(b)** followed by ^{68}Ga-grazytracer PET scan one month after CAR-T cell therapy. Subsequent ^{18}F-FDG PET scans were performed at **(c)** 1 month and **(d)** 14 months post-therapy to monitor prognosis. **(e–h)** A patient with B-cell lymphoma underwent the same imaging sequence. Reproduced from Ref. [18] © 2024 Springer Nature.

^{99m}Tc to identify patients suited for PD-L1 blockade immunotherapy [19]. In another case, they labeled the H10F peptide with ^{99m}Tc for trastuzumab treatment monitoring [20]. As-prepared ^{99m}Tc-HYNIC-H10F provided periodic monitoring of HER2 expression before, during, and after treatment. HER2 biomarkers are dynamic and change throughout the treatment process. This tumor marker adaptability provides valuable insights into the effectiveness of treatment, helping clinicians fine-tune treatment approaches for better outcomes. As a result, ^{99m}Tc-HYNIC-H10F predicted treatment outcomes 7 days earlier than tumor size detection. However, the rapid clearance of ^{99m}Tc-HYNIC-H10F limited its clinical application. To address this dilemma, in another work, the H10F peptide was further modified with PEG and then labeled with ^{99m}Tc to prepare ^{99m}Tc-HP-Ark2 [14]. After piloting the clinical study with 36 patients, it turned out ^{99m}Tc-HP-Ark2 SPECT/CT imaging reflected the HER2 status with an accuracy of 88.9% (32/36) which is much higher than ^{18}F-FDG PET/CT (27/36). It can also identify 100% of IHC (3+) breast tumors, implying great potential of SPECT in CDx.

In addition to radionuclide-based imaging methods, fluorescence (FL) imaging, and photoacoustic (PA) imaging are increasingly being integrated into the design of molecular imaging-based CDx due to its non-ionizing radiation and fast feedback. For example, Wang et al. developed a vascular endothelial growth factor (VEGF)-targeting FL CDx, BevF(ab′)2, to assess the tumor response and identify patients who benefit from gefitinib treatment [20]. Very recently, our group developed a FL/PA dual-mode CDx sensor (NIR-CE) to stratify tumors according to carboxylesterase (CE) level [21]. CE removed the acetyl group from NIR-CE, producing the intermediate NIR-CE-OH. This intermediate underwent spontaneous hydrogen atom rearrangement between the nitrogen in the indole group and the phenol hydroxyl group, ultimately enhancing FL intensity at 708 nm and PA signals at 684 nm. In double-blind screening experiments, NIR-CE successfully distinguished HepG2 (high CE levels) and MDA-MB-231 tumor (low CE levels)-bearing mice with 100% confidence (Fig. 3), confirming its potential as a CDx tool for tumor identification in CE-activated prodrug therapy.

Apart from that, Song et al. [22] designed an activated afterglow/MRI bimodal probe as a CDx tool to dynamically monitor the biomarker apurinic/apyrimidinic endonuclease 1 (APE1) during *in vivo* radiotherapy (Fig. 4(a)). APE1 is a multifunctional protein that plays a crucial role in DNA repair and redox signaling. Its expression correlates positively with radiotherapy, thus serving as a potential biomarker for monitoring and

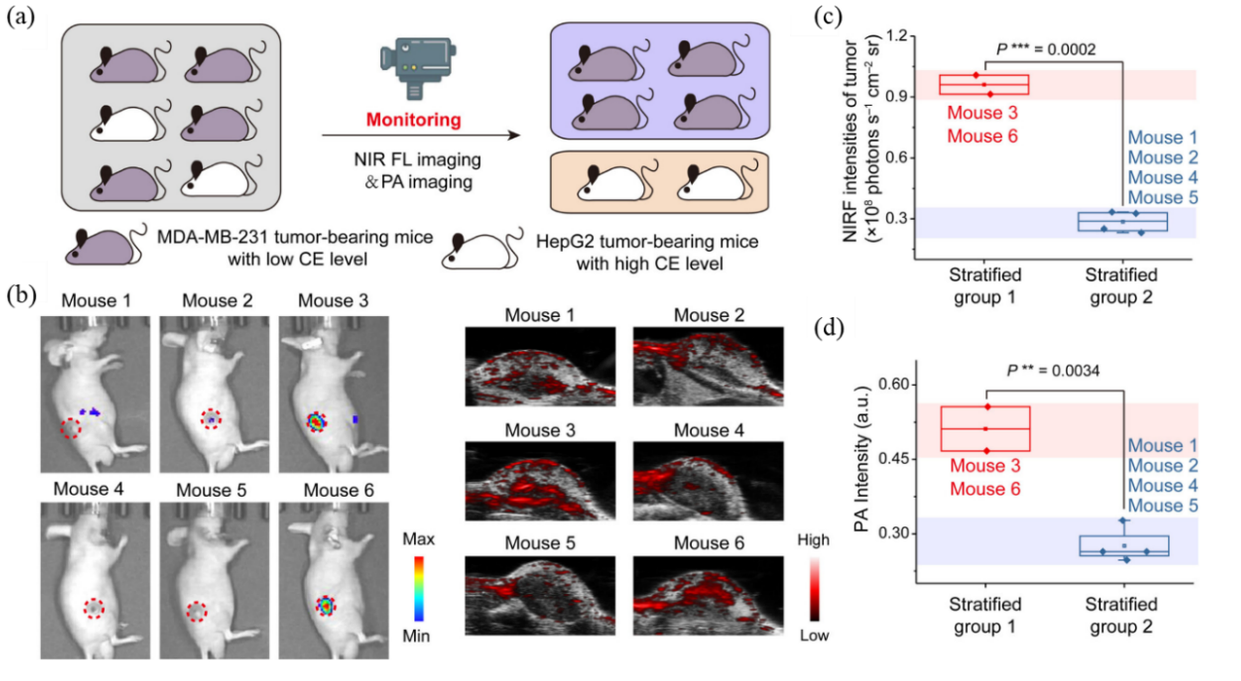

Fig. 3 CDx sensor NIR-CE distinguished MDA-MB-231 and HepG2 tumor-bearing mice via FL and PA bimodal imaging. **(a)** The scheme of the double-blind experiment. **(b)** The FL- and PA-images of mice 1–6. The quantification results of **(c)** FL intensities and **(d)** PA intensities. Reproduced with permission from Ref. [21] © 2024 Wiley-VCH GmbH.

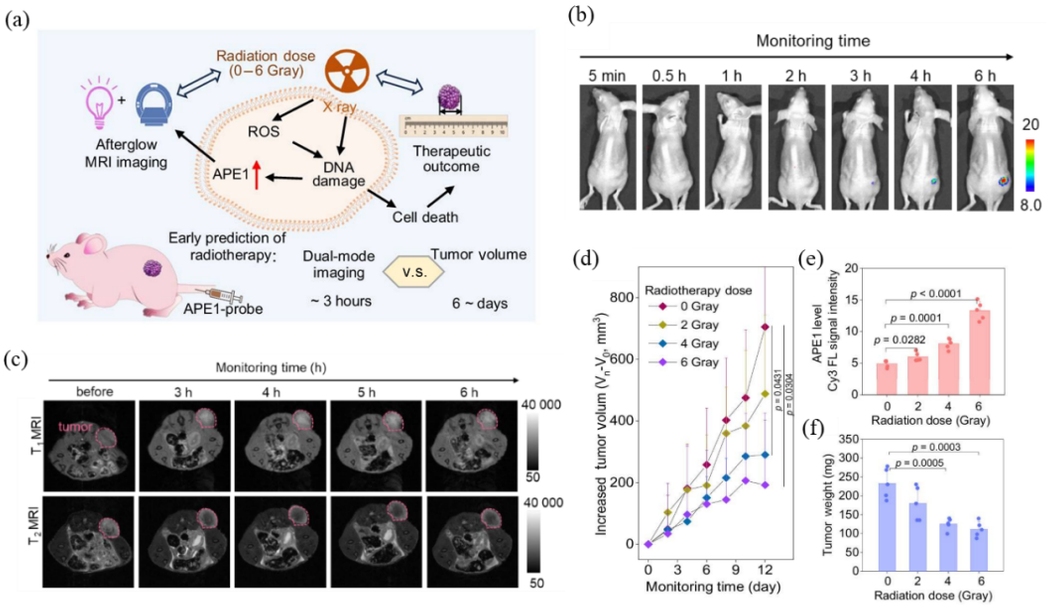

Fig. 4 APE1-responsive afterglow and MRI dual-mode probes for radiotherapy monitoring and early prediction. **(a)** A schematic illustration depicting the mechanism of the CDx process. **(b)** FL and **(c)** MR images of the mice treated with 6 Gray radiation and then intravenous injection of APE1-probe. **(d)** Tumor growth curves following varying doses of radiotherapy within 12 days. **(e)** The APE1 levels and **(f)** tumor weights tested on Day 12. Reproduced from Ref. [22] © 2024 Yue, et al.

prediction. To detect APE1, a DNA sequence containing APE1-responsive apurinic/apyrimidinic sites was designed and modified onto afterglow and ultrasmall FeMnOx nanoparticles. Through DNA hybridization, a core–shell nanostructure was formed as an APE1 nanoprobe. This probe exhibited very low limit detections: 0.009 2 U/mL for afterglow and 0.16 U/mL for MRI. By tracking APE1 levels *in vivo*, this probe offered an early prediction of radiotherapy outcomes as early as 3 h-post treatment (Figs. 4(b) and 4(c)), much earlier before visible tumor shrinkage occurs (~ 6 days, Figs. 4(d)–4(f)). Therefore, this APE1 nanoprobe served as a CDx tool for radiotherapy prediction and monitoring.

Imaging-based CTx

As medical technology continues to develop, here emerges another pivotal discipline, in vivo CTx. CTx moves beyond CDx to a more streamlined medical process that eliminates the time lag between CDx and treatment, making it a key advancement in personalized medicine. The molecular design principle of CTx sensors centers on controlled signal modulation, where the signal activation or deactivation is influenced by therapeutic processes. During treatment, as the target environment or biomarker expression changes-due to therapeutic effects such as tumor shrinkage or receptor downregulation, a precise molecular mechanism-such as a conformational change, enzymatic cleavage, or environmental sensitivity-triggers a shift in the probe's structure, leading to the release or activation of a detectable signal. This controlled signal change, often achieved through FL, PA, and MRI, reflects the treatment's impact in real-time, providing insights into the progress or effectiveness of therapy by monitoring dynamic shifts in signal intensity or patterns. We will introduce the CTx according to the activate mechanisms, which can be classified into tumor marker- or treatment-activated CTx. These molecular probe-involved CTx sensors are summarized in Table 3.

Tumor marker-activated CTx

Compared with FDA-approved CDx which mainly uses stoichiometric binding events to target cell surface receptors, CTx tends to utilize the activity-based sensing strategy to selectively monitor the tumor-specific active markers such as enzymes and other small molecular indicators (GSH, H^+, O_2). This shift involves the use of activatable probes, which respond to the dynamic environment within the tumor. For example, Jefferson Chan et al. utilized the physical organic chemistry approach to synthesize a panel of 14 GSH probes incorporating various electron-withdrawing and electron-donating groups at

Table 3 Representative CTx sensors.

Chemical structure	Stimulus	Therapy	Imaging Modalities	Ref.
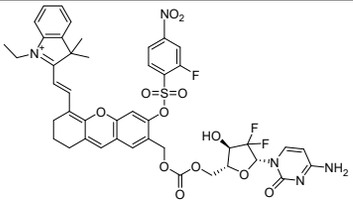	GSH	Gemcitabine	PA	[23]
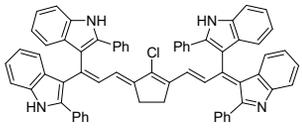	H^+/Viscosity	PTT	FL	[24]
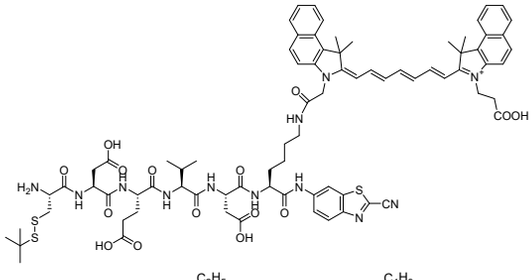	Caspase-3	PTT	FL	[25]
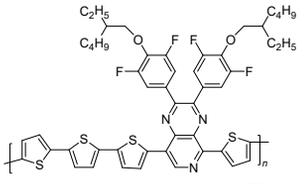	$^1O_2$	CDT (Co^{3+})	CL	[26]
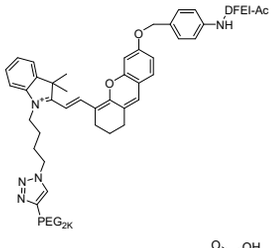	Granzyme B	Immunotherapy	FL	[27]
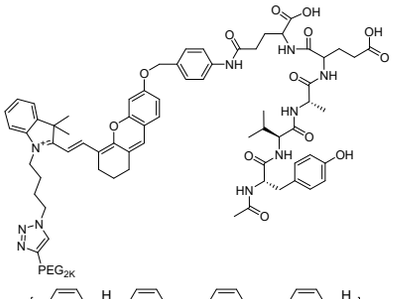	Caspase-1/GGT	Chemo-Immunotherapy	FL	[28]
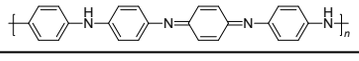	H^+	PTT/GOx	PA	[29]

Note: GSH: glutathione; PTT: photothermal therapy; GOx: glucose oxidase; CDT: chemodynamic therapy; CL: chemiluminescence; GGT: gamma-glutamyl transferase;.

the *para* and *ortho* positions to select a fine-tuned tumor-specific GSH probe (PACDx) [23]. In a double-blind experiment, mice were implanted with either U87 (low GSH) or A549 (high GSH) tumors to assess the CTx potential of PACDx. As expected, six of seven mice with greater than 95% confidence were correctly classified based on the tumor type they carried. Furthermore, after giving GSH-activated PACDx-gemcitabine prodrugs, mice with strong PA intensities showed better tumor suppression.

Apart from the molecular marker, our group synthesized an acid and viscosity cascade-responsive probe, LET-1052, to detect the mechanical marker changes during therapy (Fig. 5) [24]. In the acidic environment of tumors, the protonation of nitrogen atoms of LET-1052 led to an increase in the absorption peak at 1 052 nm, facilitating PTT under

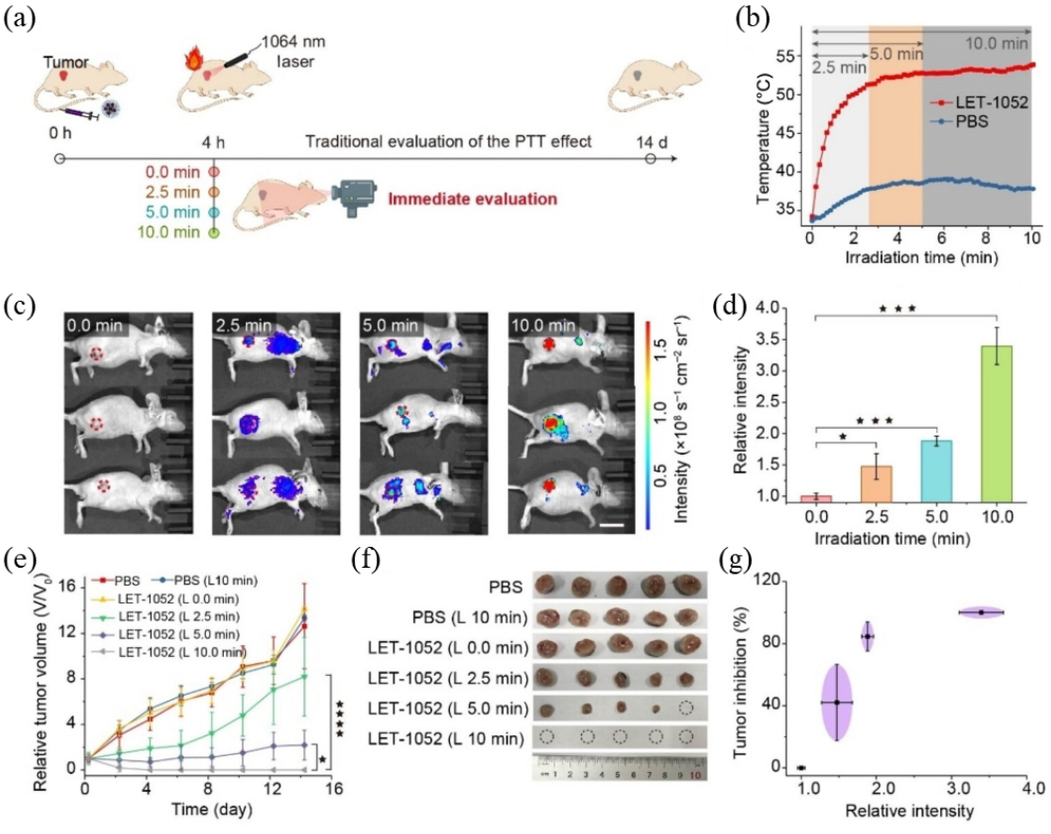

Fig. 5 The CTx role of LET-1052 by testing the PTT-induced viscosity changes. **(a)** A schematic illustration of treatment and monitoring regimen. **(b)** The temperature curves of 4T1 tumor-bearing mice after intravenous injection of PBS and the LET-1052 probe. **(c)** FL imaging of LET1052-treated mice with different durations of light irradiation and **(d)** its corresponding quantification results. **(e)** The tumor growth curves after different treatments. **(f)** The tumor images on Day 14. **(g)** The correlation between FL intensity and tumor inhibition. Reproduced with permission from Ref. [24] © 2022 Wiley-VCH GmbH.

1 064 nm excitation. Interestingly, this PTT-induced cell death increased intracellular viscosity to restrict the molecular rotation of LET-1052, resulting in enhanced FL at 684 nm. Different irradiation durations (0, 2.5, 5.0, and 10 min) at tumor lesions resulted in varying PTT doses of 0, 29.1, 74.7, and 171.9 °C min, respectively (Fig. 5(b)). As a result, the 10-min group exhibited FL intensities 2.3- and 3.4-times higher than those in the 2.5 and 0 min groups, respectively (Figs. 5(c)–5(d)). After continuing monitoring the tumor growth, a strong positive correlation between FL intensities and tumor suppression was found (Figs. 5(c)–5(g)). Compared to traditional methods for assessing tumor volume changes, this self-checking strategy provided immediate and real-time reflections of treatment efficacy, offering therapeutic efficacy evaluation results at least two weeks earlier.

Caspase-3 is the most commonly used active enzyme marker in the design of CTx for monitoring apoptosis of tumor cells, thereby reflecting the efficacy of these treatments in inducing programmed cell death. Elevated levels of caspase-3 can be utilized to active probes in many therapies, including radiotherapy [30], chemotherapy [31], photodynamic therapy (PDT) [32], and so on. Liang et al. developed a caspase-3 responsive nanoprobe (Cy-CBT) for self-evaluating PTT [25]. Cy-CBT is self-assembled into nanoparticles through the click condensation reaction to quench its FL. During PTT, the expression of caspase-3 triggers the cleavage of the DEVD peptide of Cy-CBT, which in turn activates the FL, allowing for the dynamic assessment of the therapeutic efficacy of the treatment. Sengupta et al. described a stimuli-responsive polymeric nanostructure with a polymer backbone conjugated to a cytotoxic chemotherapeutic and a caspase-3-activatable FL probe [31]. The reporter nanoparticle begins emitting a signal as early as 12 h post-chemotherapy, while significant changes in tumor volume are only observed after 6 days of treatment.

Treatment-activated CTx

Many therapeutic agents do not necessarily affect

tumor cell markers directly but instead produce cytotoxic small molecules, hyperthermia, or anticancer immune responses. In this case, the CTx's design to monitor these lethal factors represents a promising approach.

One of the most advanced and strategically designed CTx today centers on the targeted generation of reactive oxygen species (ROS), attributing to the extensive development of both ROS-based therapeutic agents and diagnostic probes. This wide array of tools enables researchers and clinicians to harness ROS in various therapeutic contexts, enhancing both the precision and effectiveness of treatments. For example, Song et al. developed core-satellite semiconducting polymer nanoparticles@cobalt hydroxide oxide (SPNs@CoOOH) to produce singlet oxygen ($^1O_2$) (Fig. 6) [26]. The cytotoxic $^1O_2$ then provided the chemical energy to the thiophene-based SPNs, enabling high-sensitivity CL emission. After intratumor injection of SPNs@CoOOH, a strong linear correlation (R^2 = 0.990) between CL intensities (measured on Day 0) and tumor inhibition rates (measured on Day 14) was found (Fig. 6(e)), validating the CTx role of SPNs@CoOOH for therapy prediction. In another case, Tan et al. loaded indocyanine green (ICG) into as-prepared upconverting covalent organic framework nanoplatforms (UCCOFs) for self-reporting PDT [33]. Interestingly, ICG was found to quench the upconversion luminescence (UCL) of UCCOFs. During PDT, ICG was decomposed by $^1O_2$, recovering the UCL signal. As a result, a highly linear correlation (R^2 = 0.997) between the tumor inhibition rate and the UCL signal intensity was found in this study, allowing tumor prediction and real-time monitoring.

In the context of PTT, there has been considerable advancement in the development of CTx tools by integrating thermos-responsive nanomaterials into PTT systems. These nanomaterials allow for the visualization of local temperature increases at the tumor site, providing real-time feedback. For example, Rosal et al. introduced an innovative application of PbS/CdS/ZnS quantum dots (QDs), which emit in the near-infrared II (NIR-II) spectrum, for temperature self-monitoring during PTT [34]. These QDs exhibit a highly sensitive and linear decrease in emission intensity as the temperature rises, enabling precise real-time monitoring of thermal dynamics within the tumor. This capability allows for the differentiation between intra-tumor and surface temperatures, ensuring fine control over temperature increments during therapy. Apart from

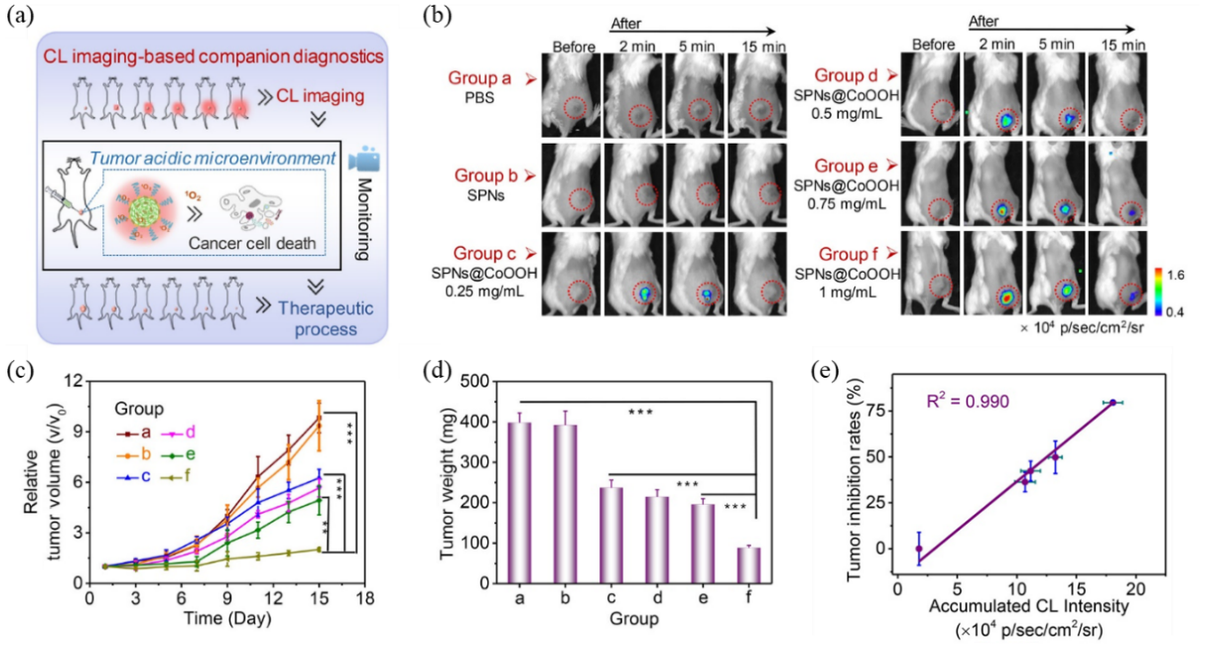

Fig. 6 (a) The scheme of CL imaging-based CTx for therapy monitoring and prediction. **(b)** The CL images within 15 min of 4T1 tumor-bearing mice after different treatments and **(c)** its tumor growth curves within 15 days. **(d)** The tumor weight measured on Day 15. **(e)** The correlation between CL intensity and tumor inhibition. Reproduced with permission from Ref. [26] © 2023 Elsevier B.V.

monitoring temperature, our group developed a CTx tool to guide PTT by fabricating a GOx-functionalized polyaniline (PANI) nanoplatform (PANITG) [35]. As GOx reacts with glucose, it amplifies the therapeutic effects by enhancing the photothermal response, and in turn, the photothermal effect boosts GOx activity, creating a self-reinforcing cycle. Additionally, PANITG's PA imaging capabilities allow real-time monitoring of tumor pH, which correlates with both the effectiveness of photothermal therapy and GOx catalytic activity at various stages, facilitating real-time activatable CTx for personalized PTT.

Another cutting-edge approach in CTx settings is metal-based therapy, which leverages the unique inherent dual functionality of imaging and therapeutic capabilities of metals and metal-based compounds to achieve highly targeted therapeutic effects. Many metal ions exhibit this dual functionality. For instance, Gadolinium (Gd) is used in MRI-guided therapy, gold (Au) in PTT and CT imaging, and iron oxide in MRI and magnetic hyperthermia, making them highly suitable for CTx applications where diagnosis and treatment occur simultaneously. Recently, Song et al. prepared Gd-oxide nanosheets with exceptional acid-responsive ability to release cytotoxic Gd ions in orthotopic hepatocellular carcinoma [35]. Freed Gd ions enhance T_1-MRI signals by increasing water molecule binding and accelerating exchange. A positive correlation between T_1-MRI intensity and tumor inhibition rates was observed. These nanosheets also allowed for the visualization of submillimeter-sized tumors (~ 0.75 mm), closely matching hematoxylin and eosin (H&E) staining results (~ 0.722 mm), making it serve as real-time CTx for treatment response and efficacy monitoring.

Conclusion and Prospects

CTx represents a significant advancement in personalized medicine, bridging the gap between CDx and therapy through real-time and integrated approaches. The continued evolution of CTx will likely be driven by interdisciplinary collaboration between scientists and clinicians. The rationale behind the development of CTx stems from several key factors.

(1) CTx is built upon the precise and sensitive detection of molecular elements, specific protein expressions, drug pharmacokinetics, and so on. As-tracked changes need to be highly specific to the disease and must also be measurable with probes. The complexity of cancer, where multiple pathways are involved, makes it difficult to pinpoint a single element that correlates with therapeutic outcomes. Thus, further refinement of pathological features will enhance reliability and improve therapy outcomes.

(2) A precision-tuned probe is significantly important for the activity-based CTx. For monitoring active therapeutic substances, a lower detection limit is generally preferred to enhance sensitivity and accuracy. However, when it comes to monitoring tumor markers, the detection limits must be carefully tailored to the specific scenario. Excessively low detection limits might fail to differentiate between tumor and normal tissue, leading to false positives or inaccuracies.

(3) When designing CTx, it is crucial to consider the relationship between the therapeutic outcome and the diagnostic tool. Ideally, this relationship should be structured as a clear upstream-downstream connection, where the diagnostic informs the therapy, and the therapy's efficacy can be measured directly by the diagnostic tool. Simple systems with minimal intermediate steps are favorable. The more steps involved, the higher the chance of introducing variables that weaken the correlation between the diagnostic data and the therapeutic outcome.

(4) CTx undergoes rigorous clinical validation to ensure its effectiveness across diverse patient populations. This process requires large-scale clinical trials, which can be both expensive and time-consuming. Thus, greater investment should be devoted to the technologies and regulatory frameworks of CTx.

CRediT Author Statement

Meng Li: investigation and writing original draft. **Yumeng Wu:** formal analysis. **Jing Lin:** conceptualization, supervision, writing–review, and editing.

Acknowledgements

This work was financially supported by the National

Natural Science Foundation of China (No. 82372116), China Postdoctoral Science Foundation (No. 2023M742404), Postdoctoral Fellowship Program of CPS Funder (No. GZB20230449), Shenzhen Science and Technology Program (Nos. JCYJ20220818095806014 and KQTD20190929172538530), and Research Team Cultivation Program of Shenzhen University (No. 2023QNT019).

Conflict of Interests

The authors declare no conflict of interest.

References

[1] A.M. Khaliq, M. Rajamohan, O. Saeed, et al. Spatial transcriptomic analysis of primary and metastatic pancreatic cancers highlights tumor microenvironmental heterogeneity. *Nature Genetics*, 2024, 56: 245−2465. https://doi.org/10.1038/s41588-024-01914-4

[2] R.E. Hynds, A. Huebner, D.R. Pearce, et al. Representation of genomic intratumor heterogeneity in multi-region non-small cell lung cancer patient-derived xenograft models. *Nature Communications*, 2024, 15: 4653. https://doi.org/10.1038/s41467-024-47547-3

[3] X. Ma, M. Mao, J. He, et al. Nanoprobe-based molecular imaging for tumor stratification. *Chemical Society Reviews*, 2023, 52(18): 6447−6496. https://doi.org/10.1039/D3CS00063J

[4] S.J. Pan, A.X. Ding, Y.S. Li, et al. Small-molecule probes from bench to bedside: Advancing molecular analysis of drug–target interactions toward precision medicine. *Chemical Society Reviews*, 2023, 52(16): 5706−5743. https://doi.org/10.1039/D3CS00056G

[5] V. Valla, S. Alzabin, A. Koukoura, et al. Companion diagnostics: State of the art and new regulations. *Biomark Insights*, 2021, 16: 11772719211047763. https://doi.org/10.1177/11772719211047763

[6] J.T. Jørgensen. Twenty-five years with companion diagnostics. *Chinese Clinical Oncology*, 2023, 12(6): 65. https://doi.org/10.21037/cco-23-96

[7] S. Liao, M. Zhou, Y. Wang, et al. Emerging biomedical imaging-based companion diagnostics for precision medicine. *iScience*, 2023, 26(8): 107277. https://doi.org/10.1016/j.isci.2023.107277

[8] E.B. Ehlerding, P. Grodzinski, W.B. Cai, et al. Big potential from small agents: Nanoparticles for imaging-based companion diagnostics. *ACS Nano*, 2018, 12(3): 2106−2121. https://doi.org/10.1021/acsnano.7b07252

[9] F. Desiere, T.S. Gutjahr, U.P. Rohr. Developing companion diagnostics for delivering personalised medicine: Opportunities and challenges. *Drug Discovery Today: Therapeutic Strategies*, 2013, 10(4): e175−e181. https://doi.org/10.1016/j.ddstr.2013.05.002

[10] H. Lee, D. Gaddy, M. Ventura, et al. Companion diagnostic ^{64}Cu-liposome positron emission tomography enables characterization of drug delivery to tumors and predicts response to cancer nanomedicines. *Theranostics*, 8(9): 2300–2312. https://doi.org/10.7150/thno.21670

[11] R. Yin, Q.P. Zhang, S.Y. Liao, et al. Medical imaging-based companion diagnostics for solid tumors. *EngMedicine*, 2024, 1(1): 100009. https://doi.org/10.1016/j.engmed.2024.100009

[12] S. Alkindi, V. Panjwani, S. Al-Rahbi, et al. Iron overload in patients with heavily transfused sickle cell disease-correlation of serum ferritin with cardiac T2* MRI (CMRTools), liver T2* MRI, and R2-MRI (ferriscan®). *Frontiers in Medicine*, 2021, 8: 731102. https://doi.org/10.3389/fmed.2021.731102

[13] R.J. Theilmann, R. Borders, T.P. Trouard, et al. Changes in water mobility measured by diffusion MRI predict response of metastatic breast cancer to chemotherapy. *Neoplasia*, 2004, 6(6): 831−837. https://doi.org/10.1593/neo.03343

[14] M.W. Ah-See, A. Makris, N.J. Taylor, et al. Early changes in functional dynamic magnetic resonance imaging predict for pathologic response to neoadjuvant chemotherapy in primary breast cancer. *Clinical Cancer Research*, 2008, 14(20): 6580−6589. https://doi.org/10.1158/1078-0432.ccr-07-4310

[15] B.A. Hoeben, E.G. Troost, P.N. Span, et al. 18F-FLT PET during radiotherapy or chemoradiotherapy in head and neck squamous cell carcinoma is an early predictor of outcome. *Journal of Nuclear Medicine*, 2013, 54(4): 532–540. https://doi.org/10.2967/jnumed.112.105999

[16] K. McLarty, B. Cornelissen, Z. Cai, et al. Micro-SPECT/CT with 111In-DTPA-pertuzumab sensitively detects trastuzumab-mediated HER2 downregulation and tumor response in athymic mice bearing MDA-MB-361 human breast cancer xenografts. *Journal of Nuclear Medicine*, 2009, 50(8): 1340−1348. https://doi.org/10.2967/jnumed.109.062224

[17] G. Gebhart, L.E. Lamberts, Z. Wimana, et al. Molecular imaging as a tool to investigate heterogeneity of advanced HER2-positive breast cancer and to predict patient outcome under trastuzumab emtansine (T-DM1): The ZEPHIR trial. *Annals of Oncology*, 2016, 27(4): 619−624. https://doi.org/10.1093/annonc/mdv577

[18] X.L. Shen, H.Y. Zhou, X. Zhou, et al. 68Ga-grazytracer PET for noninvasive assessment of response to immunotherapy in solid tumors and lymphomas: A phase 1/2 clinical trial. *Nature Communications*, 2024, 15: 8791. https://doi.org/10.1038/s41467-024-53197-2

[19] H. Gao, Y. Wu, J. Shi, et al. Nuclear imaging-guided PD-L1 blockade therapy increases effectiveness of cancer immunotherapy. *Journal for Immunotherapy of Cancer*, 2020, 8(2): e001156. https://doi.org/10.1136/jitc-2020-001156

[20] Y. Wu, L.Q. Li, Z.H. Wang, et al. Imaging and monitoring HER2 expression in breast cancer during trastuzumab therapy with a peptide probe 99mTc-HYNIC-H10F. *European Journal of Nuclear Medicine and Molecular Imaging*, 2020, 47(11): 2613−2623. https://doi.org/10.1007/s00259-020-04754-6

[21] B. Li, H. Liu, M. Zhao, et al. Carboxylesterase activatable molecular probe for personalized treatment guidance by analyte-induced molecular transformation. *Angewandte Chemie*, 2024, 63(31): e202404093. https://doi.org/10.1002/anie.202404093

[22] Yue, R. Y., Li, Z., Liu, H. Y., Wang, Y. J., Li, Y. H., Yin, R., Yin, B. L., Qian, H. S., Kang, H., Zhang, X. B. et al. Imaging-guided companion diagnostics in radiotherapy by monitoring APE1 activity with afterglow and MRI imaging. *Nature Communications*, 2024, 15: 6349. https://doi.org/10.1038/s41467-024-50688-0

[23] M.Y. Lucero, J. Chan. Photoacoustic imaging of elevated glutathione in models of lung cancer for companion diagnostic applications. *Nature Chemistry*, 2021, 13(12): 1248−1256. https://doi.org/10.1038/s41557-021-00804-0

[24] B.H. Li, H.K. Liu, Y.L. He, et al. A “self-checking” pH/viscosity-activatable NIR-II molecule for real-time

evaluation of photothermal therapy efficacy. *Angewandte Chemie*, 2022, 61(16): e202200025. https://doi.org/10.1002/anie.202200025

[25] Y. Wang, W. Du, T. Zhang, et al. A self-evaluating photothermal therapeutic nanoparticle. *ACS Nano*, 2020, 14(8): 9585−9593. https://doi.org/10.1021/acsnano.9b10144

[26] C. Lu, Z. Li, N. Wu, et al. Tumor microenvironment-tailored nanoplatform for companion diagnostic applications of precise cancer therapy. *Chem*, 2023, 9(11): 3185−3211. https://doi.org/10.1016/j.chempr.2023.06.011

[27] S. He, J. Li, Y. Lyu, et al. Near-infrared fluorescent macromolecular reporters for real-time imaging and urinalysis of cancer immunotherapy. *Journal of the American Chemical Society*, 2020, 142(15): 7075−7082. https://doi.org/10.1021/jacs.0c00659

[28] X.Z. Wang, S.S. He, P.H. Cheng, et al. A dual-locked tandem fluorescent probe for imaging of pyroptosis in cancer chemo-immunotherapy. *Advanced Materials*, 2023, 35(10): 2206510. https://doi.org/10.1002/adma.202206510

[29] J. Wu, Y. Zhang, K. Jiang, et al. Enzyme-engineered conjugated polymer nanoplatform for activatable companion diagnostics and multistage augmented synergistic therapy. *Advanced Materials*, 2022, 34(18): e2200062. https://doi.org/10.1002/adma.202200062

[30] Q. Fu, H. Feng, L. Su, et al. An activatable hybrid organic-inorganic nanocomposite as early evaluation system of therapy effect. *Angewandte Chemie*, 2022, 61(7): e202112237. https://doi.org/10.1002/anie.202112237

[31] A. Kulkarni, P. Rao, S. Natarajan et al. Reporter nanoparticle that monitors its anticancer efficacy in real time. *Proceedings of the National Academy of Sciences of the United States of America*, 2016, 113(15): E2104−E2113. https://doi.org/10.1073/pnas.1603455113

[32] L. Zhang, J. Lei, F. Ma, et al. A porphyrin photosensitized metal-organic framework for cancer cell apoptosis and caspase responsive theranostics. *Chemical Communications*, 2015, 51(54): 10831−10834. https://doi.org/10.1039/C5CC03028E

[33] P. Wang, F. Zhou, K. Guan, et al. *In vivo* therapeutic response monitoring by a self-reporting upconverting covalent organic framework nanoplatform. *Chemical Science*, 2019, 11(5): 1299–1306. https://doi.org/10.1039/C9SC04875H

[34] B. del Rosal, E. Carrasco, F.Q. Ren, et al. Infrared-emitting QDs for thermal therapy with real-time subcutaneous temperature feedback. *Advanced Functional Materials*, 2016, 26(33): 6060−6068. https://doi.org/10.1002/adfm.201601953

[35] C. Zhang, X. Wang, J. Xu, et al. Ultrathin Gd-oxide nanosheet as ultrasensitive companion diagnostic tool for MR imaging and therapy of submillimeter microhepatocellular carcinoma. *Nano Letters*, 2024, 24(35): 11002−11011. https://doi.org/10.1021/acs.nanolett.4c03078